

ORIGINAL ARTICLE

Open Access



# $^{18}\text{F}$ -FDG PET/CT-based radiomics nomogram could predict bone marrow involvement in pediatric neuroblastoma

Lijuan Feng<sup>1†</sup>, Xu Yang<sup>1†</sup>, Xia Lu<sup>1</sup>, Ying Kan<sup>1</sup>, Chao Wang<sup>2</sup>, Dehui Sun<sup>1</sup>, Hui Zhang<sup>3</sup>, Wei Wang<sup>1\*</sup> and Jigang Yang<sup>1\*</sup>

## Abstract

**Objective:** To develop and validate an  $^{18}\text{F}$ -fluorodeoxyglucose (FDG) positron emission tomography/computed tomography (PET/CT)-based radiomics nomogram for non-invasively prediction of bone marrow involvement (BMI) in pediatric neuroblastoma.

**Methods:** A total of 133 patients with neuroblastoma were retrospectively included and randomized into the training set ( $n = 93$ ) and test set ( $n = 40$ ). Radiomics features were extracted from both CT and PET images. The radiomics signature was developed. Independent clinical risk factors were identified using the univariate and multivariate logistic regression analyses to construct the clinical model. The clinical-radiomics model, which integrated the radiomics signature and the independent clinical risk factors, was constructed using multivariate logistic regression analysis and finally presented as a radiomics nomogram. The predictive performance of the clinical-radiomics model was evaluated by receiver operating characteristic curves, calibration curves and decision curve analysis (DCA).

**Results:** Twenty-five radiomics features were selected to construct the radiomics signature. Age at diagnosis, neuron-specific enolase and vanillylmandelic acid were identified as independent predictors to establish the clinical model. In the training set, the clinical-radiomics model outperformed the radiomics model or clinical model (AUC: 0.924 vs. 0.900, 0.875) in predicting the BMI, which was then confirmed in the test set (AUC: 0.925 vs. 0.893, 0.910). The calibration curve and DCA demonstrated that the radiomics nomogram had a good consistency and clinical utility.

**Conclusion:** The  $^{18}\text{F}$ -FDG PET/CT-based radiomics nomogram which incorporates radiomics signature and independent clinical risk factors could non-invasively predict BMI in pediatric neuroblastoma.

**Keywords:** Neuroblastoma, Positron emission tomography/computed tomography, Radiomics, Nomogram

## Key points

- Radiomics signature is valuable in the non-invasively diagnosis of bone marrow involvement.
- Age, NSE and VMA are the independent predictors of bone marrow involvement
- The nomogram incorporating radiomics signature and independent clinical risk factors improves predictive performance.

<sup>†</sup>Lijuan Feng and Xu Yang contributed equally to this work

\*Correspondence: 18611245486@163.com; yangjigang@ccmu.edu.cn

<sup>1</sup> Department of Nuclear Medicine, Beijing Friendship Hospital, Capital Medical University, 95 Yong An Road, Xi Cheng District, Beijing 100050, China  
Full list of author information is available at the end of the article

## Introduction

Neuroblastoma is a malignant neuroectodermal tumor that originated from cells of the neural crest and is the most common extracranial solid malignant tumor of childhood [1, 2]. About 50% of neuroblastoma patients had metastasis at the time of initial diagnosis, which is frequently associated with unsatisfactory outcomes. The bone marrow is the most common site of metastasis in neuroblastoma [3], and the spread of tumor cells to bone marrow is a grim prognostic factor in neuroblastoma patients [4]. The prognosis is significantly better in those without bone marrow involvement (BMI) than in those with BMI [5, 6]. Moreover, BMI is one of the most important diagnostic criteria and an important risk factor for staging according to the International Neuroblastoma Staging System (INSS) and the International Neuroblastoma Risk Group staging system [7–9]. Therefore, establishing an early predictive model for BMI in neuroblastoma patients is crucial for prognosis and the decision of treatment strategy.

According to the recommendations of the INSS, the cytology of aspirates and histology of biopsies are the gold standard with which to assess BMI in patients with neuroblastoma [5, 7, 8]. Considering that most neuroblastoma patients are children, the bone marrow aspirates and biopsies must be performed only by experienced health care providers who have been well-trained in the technique [10]. However, as invasive methods, the aspirates or biopsies may cause adverse events such as hemorrhage, infection and persistent pain. Moreover, bone marrow aspirates or biopsies had higher health-care costs for the method, including pathology, sedation, anesthesia and surgical suite time [11]. Because of these limitations, better non-invasive computational tools should be developed that can effectively identify neuroblastoma patients with BMI.

Radiomics analysis converts medical images into mineable high-dimensional data by extracting innumerable quantitative features with high-throughput computing [12]. Once the high-dimension feature data describing quantitative attributes of volumes of interest is available, artificial intelligence, machine learning, or statistical approaches can be used to build classifier or regression modeling for disease detection, diagnosis, evaluation of prognosis and prediction of treatment response.

In recent years,  $^{18}\text{F}$ -fluorodeoxyglucose (FDG) positron emission tomography/computed tomography (PET/CT) has been used for the evaluation of BMI and is very helpful in evaluating the BMI in many malignancies [13, 14].  $^{18}\text{F}$ -FDG PET/CT-based texture image features may provide predictive and prognostic biomarkers which performed better than standardized uptake value parameters, metabolic tumor volume and total lesion glycolysis

in lung cancer [15]. Although  $^{18}\text{F}$ -FDG PET/CT texture analyses have been applied as a new method for differentiating BMI in lymphoma [16], there has been no study about radiomics based on  $^{18}\text{F}$ -FDG PET/CT used for the prediction of BMI in pediatric neuroblastoma. Therefore, the present study aimed to develop and validate a radiomics nomogram that integrated the radiomics signature and the independent clinical risk factors for non-invasively prediction of BMI in pediatric patients with neuroblastoma.

## Materials and methods

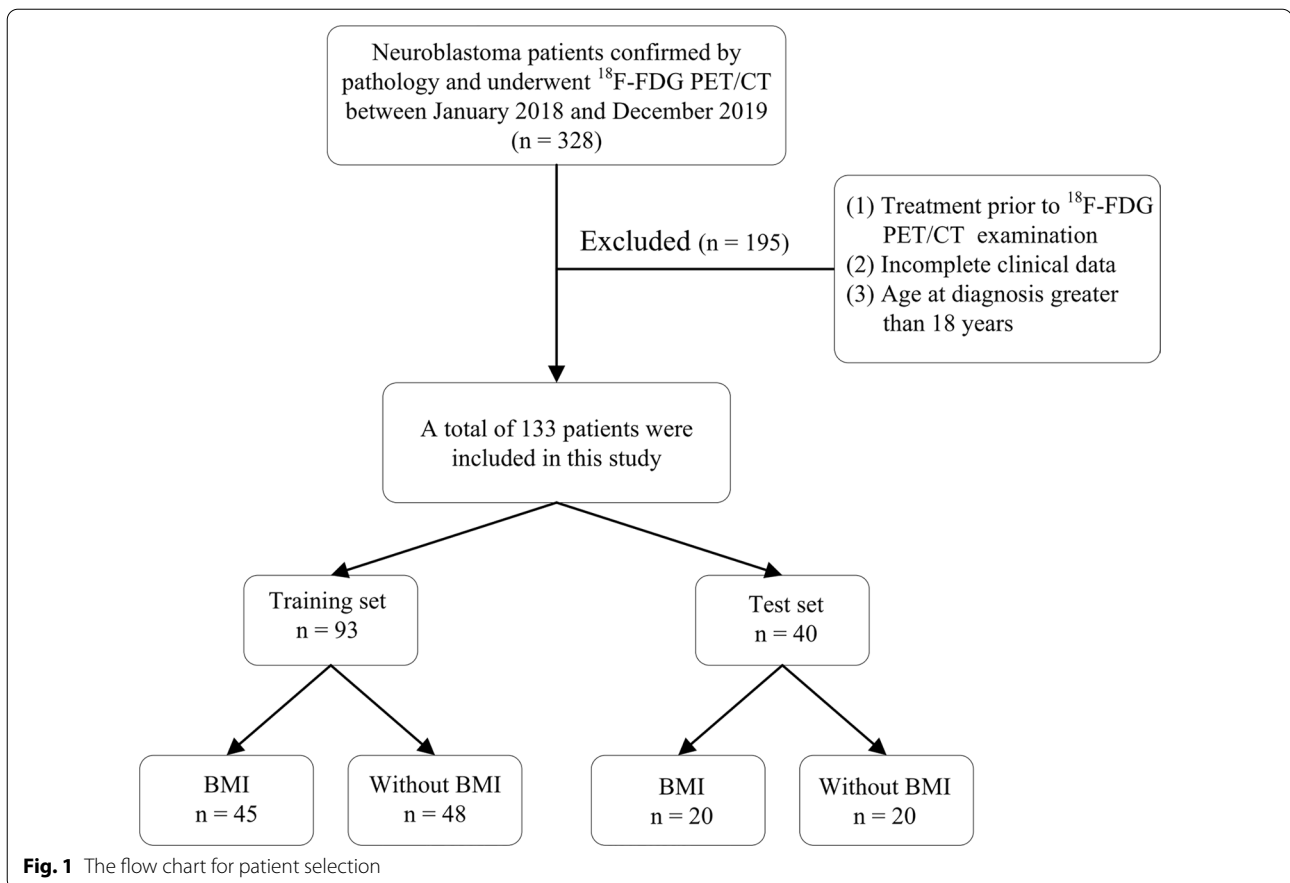
### Patients

This retrospective study was approved by the institutional review board and waived the requirement for written informed consent.

We retrospectively included a cohort of 328 patients who underwent  $^{18}\text{F}$ -FDG PET/CT in our institution with pathologically confirmed neuroblastoma between January 2018 and December 2019. The inclusion criteria consisted of (1) patients with neuroblastoma who underwent bone marrow aspirates or biopsies and were assessed BMI using morphologic criteria in conjunction with appropriate antibodies; (2)  $^{18}\text{F}$ -FDG PET/CT scan performed within 30 days before the bone marrow aspirates or biopsies. The exclusion criteria included the following: (1) patients who received tumor-related treatments such as chemotherapy, radiotherapy and surgical excision prior to  $^{18}\text{F}$ -FDG PET/CT examination; (2) patients with incomplete clinical data; (3) patients were greater than 18 years of age at diagnosis. Finally, a total of 133 patients (58 males and 75 females; median age, 3.2 years; range, 1.7–4.7 years) were retrospectively included in this study. According to the result of bone marrow aspirates or biopsies, there were 65 patients with BMI and 68 patients without BMI. The flow chart for patient selection is shown in Fig. 1.

Stratified sampling according to the BMI stratification was implemented to balance the positive and negative cases, and the final 133 cases were randomly divided into the training set and test set according to a ratio of 7:3, which resulted in 93 cases being divided into the training set and 40 cases being divided into the test set.

The baseline data of each patient were obtained by reviewing the medical records, which included the following aspects: (1) clinical information, (2) laboratory indicators, (3) PET metabolic parameters, and (4) pathological-related information. We defined these data as clinical characteristics. Laboratory indicators including neuron-specific enolase (NSE), serum ferritin, lactate dehydrogenase (LDH), urine vanillylmandelic acid (VMA) and homovanillic acid (HVA) were acquired within two weeks before therapy.



### PET/CT imaging acquisition

All patients in the cohort underwent whole body  $^{18}\text{F}$ -FDG PET/CT (Biograph mCT-64 PET/CT; Siemens, Knoxville) scans according to European Association of Nuclear Medicine guidelines for tumor imaging [17, 18]. Patients were instructed to ban from intense exercises for at least 24 h before PET/CT scan and fast at least 6 h before  $^{18}\text{F}$ -FDG injection. A mean dose of 3 mCi (mean 0.14 mCi/kg) was administrated considering the patients are children. A low-dose CT scan (CT scanning parameters: tube voltage 120 keV, thickness 2 mm, matrix size  $512 \times 512$ ) for viewing anatomic structures and attenuation correction was performed an hour after the injection. PET scan with three-dimension image mode and 2 min per bed setting followed immediately after CT acquisition. PET images were reconstructed with the time-of-flight ordered subsets-expectation maximization algorithm. All corrections for quantitative interpretation, including detector sensitivity normalization, dead time, random, scatter, attenuation and decay correction were applied during reconstruction. A Gaussian smoothing filter with a full width at half-maximum of 5 mm was applied to the PET images. The PET images' parameters

were as follows: pixel size  $4.07 \text{ mm} \times 4.07 \text{ mm}$ , 3 mm slice thickness, and matrix size  $200 \times 200$ .

### Tumor segmentation, radiomics features extraction and selection

Image segmentation was performed semi-automatically with a commonly used open-source software (3D Slicer, Version 4.10.1) by reader 1 (W.W. with 7 years of experience in pediatric oncologic radiology). An example of ROI segmentation is shown in Fig. 2. The intraclass correlation coefficient (ICC) was used to assess the reproducibility of the selected features. A total of 30 cases (15 with BMI and 15 without BMI) of CT images and PET images randomly selected from the whole cohort were independently performed repeat segmentation by reader 1 and reader 2 (Y.K. with 10 years of experience in pediatric oncologic radiology). The readers were blinded to the clinical information when performing the segmentation.

Radiomics features were extracted from both CT and PET images using Pyradiomics in Python (version 3.7.8), an open-source python package for the extraction of radiomics features from medical imaging. A fixed bin width (0.3 standardized uptake value for PET image and

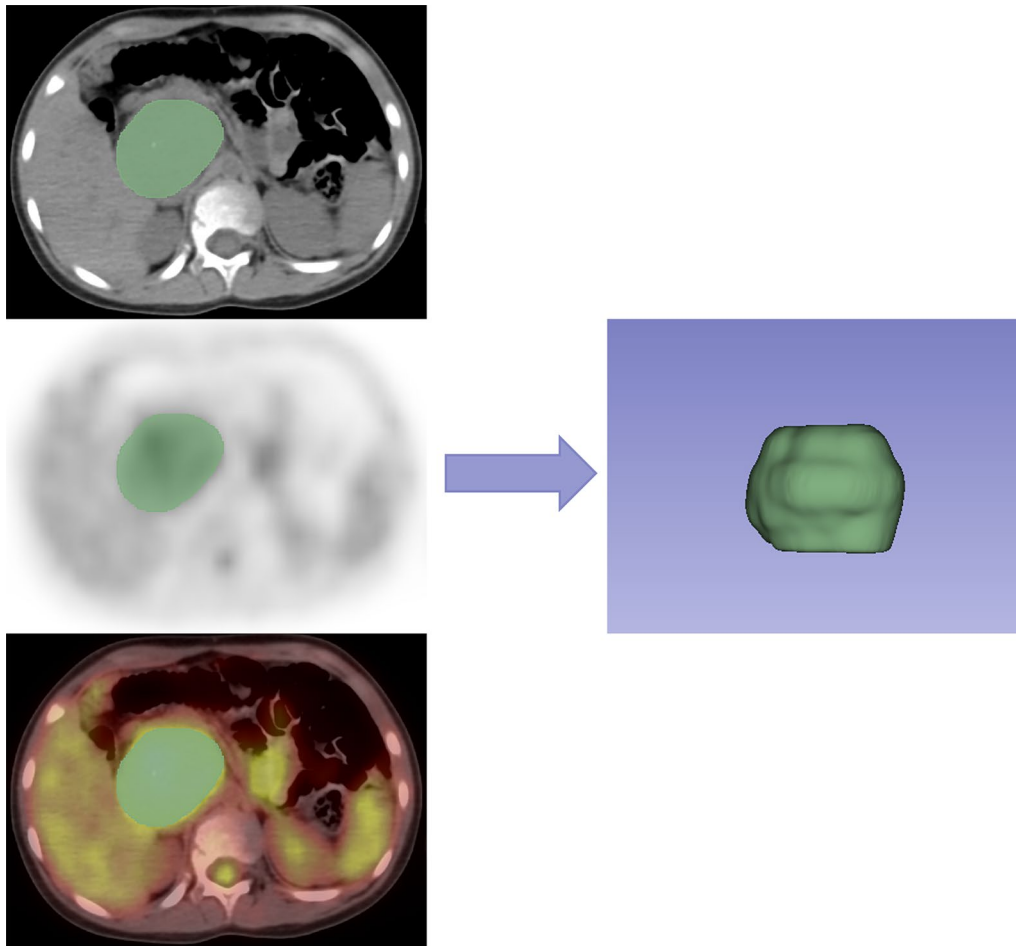


**Fig. 2** Schematic representation of the tumor segmentation by 3D Slicer

25 Hounsfield Units [HUs] for CT image) had been chosen to discretize gray value discretization for texture features extraction [19, 20]. Furthermore, filters including wavelet, square, and logarithm et al. were applied to the original CT and PET images for calculating high-dimensional features.

The features with ICC > 0.8 were considered reliable and maintained for subsequent analysis [21–23]. Then, the Pearson's correlation coefficients and Spearman's rank correlation coefficient were calculated to examine redundant and collinear features, and features with mutual correlation coefficients > 0.9 were removed [24]. Finally, the least absolute shrinkage and selection operator (LASSO) regression with fivefold cross-validation was applied for feature selection.

#### **Radiomics model, clinical model and radiomics nomogram construction and evaluation**

Using the most optimal features to construct the radiomics signature. The radiomics score (Rad score) was

calculated for each patient via the combination of the selected features with their respective weight coefficients.

The univariate logistic regression analysis was used to assess the difference in clinical characteristics between BMI and without BMI in the training set. Then, variables with  $p < 0.05$  in the univariate logistic regression analysis were applied to multivariate logistic regression analysis to elucidate the independent clinical risk factors. Meanwhile, multivariate logistic regression analysis was applied to build the clinical model was built based on the independent clinical risk factors.

The clinical-radiomics model, which incorporated the independent clinical risk factors and Rad score, was constructed using multivariable logistic regression analysis and finally presented as a radiomics nomogram in the training set. Logistic regression is a classical statistical model that internally has a linear regression, which is topped up by a sigmoid function such that the output of the model is a probability estimate between 0 and 1 [25].

The predictive performance of the clinical-radiomics model was evaluated by receiver operating characteristic (ROC) curves, calibration curves, and decision curve analysis (DCA). A calibration curve, obtained by plotting the actual probability against the nomogram-predicted probability, was used to evaluate the calibration of the nomogram. DCA was employed to evaluate the clinical utility of the radiomics nomogram.

Moreover, we applied two other machine learning methods, naive bayes and neural network, to build clinical-radiomics models, and then compared the predictive performance of the models obtained by each machine learning method based on such matrices as the area under the curve (AUC), accuracy, precision, F1-score and recall.

### Statistical analysis

Categorical variables were expressed as counts (n) and percentages (%), while continuous variables were expressed as mean values  $\pm$  standard deviation or medians with the interquartile ranges. Statistical analyses were performed using R (version 4.0.3) and IBM SPSS Statistics (version 26.0). Two-sided with  $p < 0.05$  was considered statistically significant. Univariate analysis was used to compare differences in the clinical factors between the training and test sets, using the independent t-test or Mann–Whitney U test for quantitative data, and the chi-squared test for categorical variables. Clinical independent predictors were screened using univariate and multivariate logistic regression analysis. The DeLong test was used to compare the AUC values of different models. The nomogram and calibration curve were depicted using the “rms (R)” package. DCA was performed using the “rmda (R)” package.

## Results

### Patient characteristics

The clinical characteristics of the patients in the training and test sets were summarized in Table 1. Univariate analysis indicated that there were no significant differences in all of these clinical factors between training and test sets. The complete dataset is available in Additional file 1.

### Feature selection and radiomics signature development

A total of 2632 radiomics features were extracted and the definition complies with Imaging Biomarker Standardization Initiative [26]. After assessing the robustness, 1016 out of 2632 features were retained for model building, with ICC  $> 0.8$ . One hundred and seventy-one features were identified as independent after Pearson's correlation and Spearman's rank correlation analysis. Eventually, twenty-five predictive radiomics features

were chosen to generate the radiomics signature by LASSO regression. Figure 3 showed the selection of radiomics features using the LASSO regression. The detail of the 25 radiomics features selected by LASSO (Additional file 2: Fig. 1) and the formula for the Rad score were described in the Additional file. The Rad score was statistically significant in the training set ( $p < 0.001$ ) and test set ( $p < 0.001$ ) between with BMI and without BMI patients. Figure 4 showed the Rad score for each patient, and most patients with BMI had a higher Rad score than those without BMI. It indicated that the Rad score can be a good differentiator for neuroblastoma patients with or without BMI.

### Construction of the clinical model and radiomics nomogram

Among all patients' clinical characteristics which excluded pathological-related information, nine significant predictors including age at diagnosis, gender, maximum diameter, NSE, ferritin, LDH, VMA, metabolic tumor volume and total lesion glycolysis were identified by univariate regression analysis. Age at diagnosis, NSE and VMA were identified as independent predictors of BMI by multivariate logistic regression analysis (Table 2). The AUC of the clinical model constructed by the three independent predictors of BMI was 0.875 (95% confidence interval [CI], 0.806–0.944) and 0.910 (95% CI, 0.821–0.999) in the training and test sets, respectively.

The Rad score, age at diagnosis, NSE and VMA were incorporated into the radiomics nomogram (Fig. 5A). The calibration curves demonstrated well consistency between the nomogram prediction and actual BMI in both the training and test sets (Fig. 5B, C). The radiomics nomogram achieved good predictive performance with AUCs of 0.924 (95% CI: 0.850–0.968) in the training set and 0.925 (95% CI: 0.796–0.984) in the test set.

Figure 6 showed the comparison of ROC performance between the radiomics models, clinical model and clinical-radiomics model in the training set and the test set. In the training set, the radiomics nomogram outperformed the radiomics model or clinical model (AUC: 0.924 vs. 0.900, 0.875;  $p = 0.160$ , 0.035), which was then confirmed in the test set (AUC: 0.925 vs. 0.893, 0.910;  $p = 0.349$ , 0.732). The DCA for the different models in the training and test sets were shown in Fig. 7. It demonstrated that the radiomics nomogram resulted in higher overall net benefits than either the radiomics model or the clinical model alone.

The results of the predictive performance of the clinical-radiomics model by the different machine learning methods in the training and test sets are described in the Additional file (Additional file 2: Table 1).

**Table 1** Characteristics of patients with neuroblastoma in the training set and test set

Characteristics	All Patients (n = 133)	Training set (n = 93)	Test set (n = 40)	p value
Age at diagnosis (years)	3.2 (1.7–4.7)	2.8 (1.4–4.7)	3.4 (2.0–4.7)	0.520
Gender				0.866
Female	75 (54.7%)	52 (54.8%)	23 (54.5%)	
Male	58 (45.3%)	41 (45.2%)	17 (45.5%)	
BMI				0.865
Yes	65 (48.9%)	45 (48.4%)	20 (50.0%)	
No	68 (51.1%)	48 (51.6%)	20 (50.0%)	
Maximum diameter(cm)	9.5 ± 3.9	9.3 ± 3.6	10.0 ± 4.6	0.373
MYCN Status				0.845
Amplified	22 (17.3%)	15 (16.7%)	7 (18.2%)	
Not Amplified	111 (82.7%)	78 (83.3%)	33 (81.8%)	
11q Aberration				0.575
Yes	55 (41.0%)	37 (45.2%)	18 (34.5%)	
No	78 (59.0%)	56 (54.8%)	22 (65.5%)	
1p Aberration				0.598
Yes	52 (41.0%)	35 (41.7%)	17 (40.0%)	
No	81 (59.0%)	58 (58.3%)	23 (60.0%)	
INSS Stage				0.435
1, 2, 3, 4S	43 (30.9%)	32 (31.0%)	11 (30.9%)	
4	90 (69.1%)	61 (69.0%)	29 (69.1%)	
COG Risk Stratification				0.540
Low, Intermediate	45 (32.4%)	33 (31.0%)	12 (34.5%)	
High	88 (67.6%)	60 (69.0%)	28 (65.5%)	
NSE (ng/mL)	237.5 (64.5–631.5)	217.9 (61.7–532.3)	315.3 (72.9–798.6)	0.290
Ferritin (ng/mL)	214.5 (72.8–295.8)	232.4 (91.2–303.5)	153.6 (64.6–288.6)	0.421
LDH (U/L)	578.0 (339.5–1038.0)	567.0 (339.5–904.5)	656.5 (342.0–1184.5)	0.589
VMA (μmol/L)	162.5 (46.2–501.8)	162.5 (49.8–552.6)	162.5 (32.2–473.3)	0.937
HVA (μmol/L)	36.4 (14.2–92.3)	36.4 (13.8–91.4)	36.4 (20.4–186.1)	0.595
SUVmax	5.4 (4.0–7.8)	5.2 (4.0–8.6)	5.8 (4.0–7.6)	0.941
SUVmean	2.0 (1.6–2.6)	2.0 (1.6–2.6)	2.2 (1.6–2.6)	0.669
MTV (mL)	130.3 (52.5–292.5)	130.3 (52.4–266.5)	131.8 (54.4–364.6)	0.772
TLG	269.5 (95.5–651.4)	248.0 (96.7–524.1)	296.8 (86.2–854.0)	0.662

*BMI* Bone marrow involvement, *COG* Children's Oncology Group, *HVA* Homovanillic acid, *INSS* International Neuroblastoma Staging System, *LDH* Serum lactate dehydrogenase, *MTV* Metabolic tumor volume, *NSE* Neuron-specific enolase, *TLG* Total lesion glycolysis, *VMA* Vanillylmandelic acid

## Discussion

Initial evaluation of BMI in patients with neuroblastoma had a crucial influence on the patient's prognosis, clinical decision-making and further management. In the present study, we constructed an <sup>18</sup>F-FDG PET/CT-based radiomics nomogram for the first time as a non-invasive method to predict BMI in pediatric patients with neuroblastoma. The radiomics nomogram incorporating the age at diagnosis, NSE, VMA and Rad score had an excellent predictive performance in both the training and test sets, with an AUC of 0.924 and 0.925, respectively.

Cytology of aspirates and histology of biopsies have been the gold standard with which to assess neuroblastoma disease in bone marrow for many years [6].

However, bone marrow aspirates and biopsies have a significant risk for pediatric patients that entails a multistep process with technical challenges and diagnostic complexity [27]. Radiomics is an emerging field, that has developed rapidly in recent years with the development of precision medicine [28]. Radiomics uses many automated data characterization algorithms to convert images of the ROI into quantitative high-throughput features, which radiologists cannot do with the naked eye [29]. By analyzing and calculating the quantitative features extracted from medical images to reflect information about tumor biology and microenvironment, it can elaborate on intra-tumor heterogeneity more effectively and accurately. It has become a useful imaging

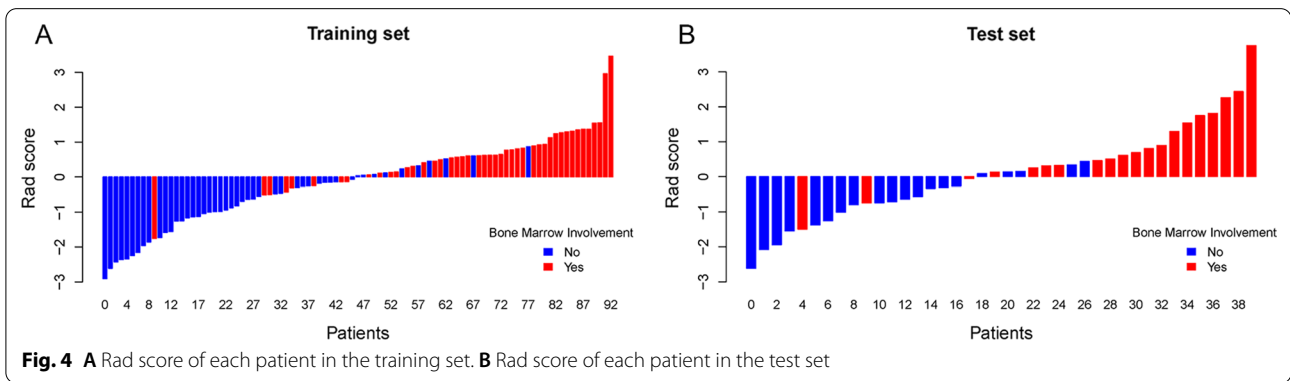
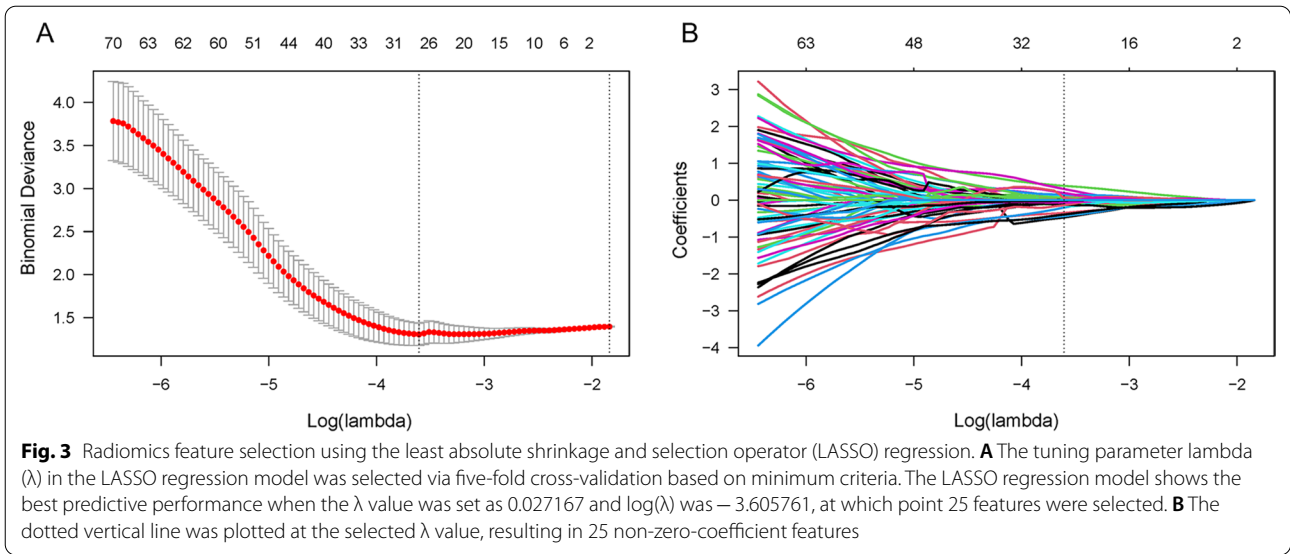
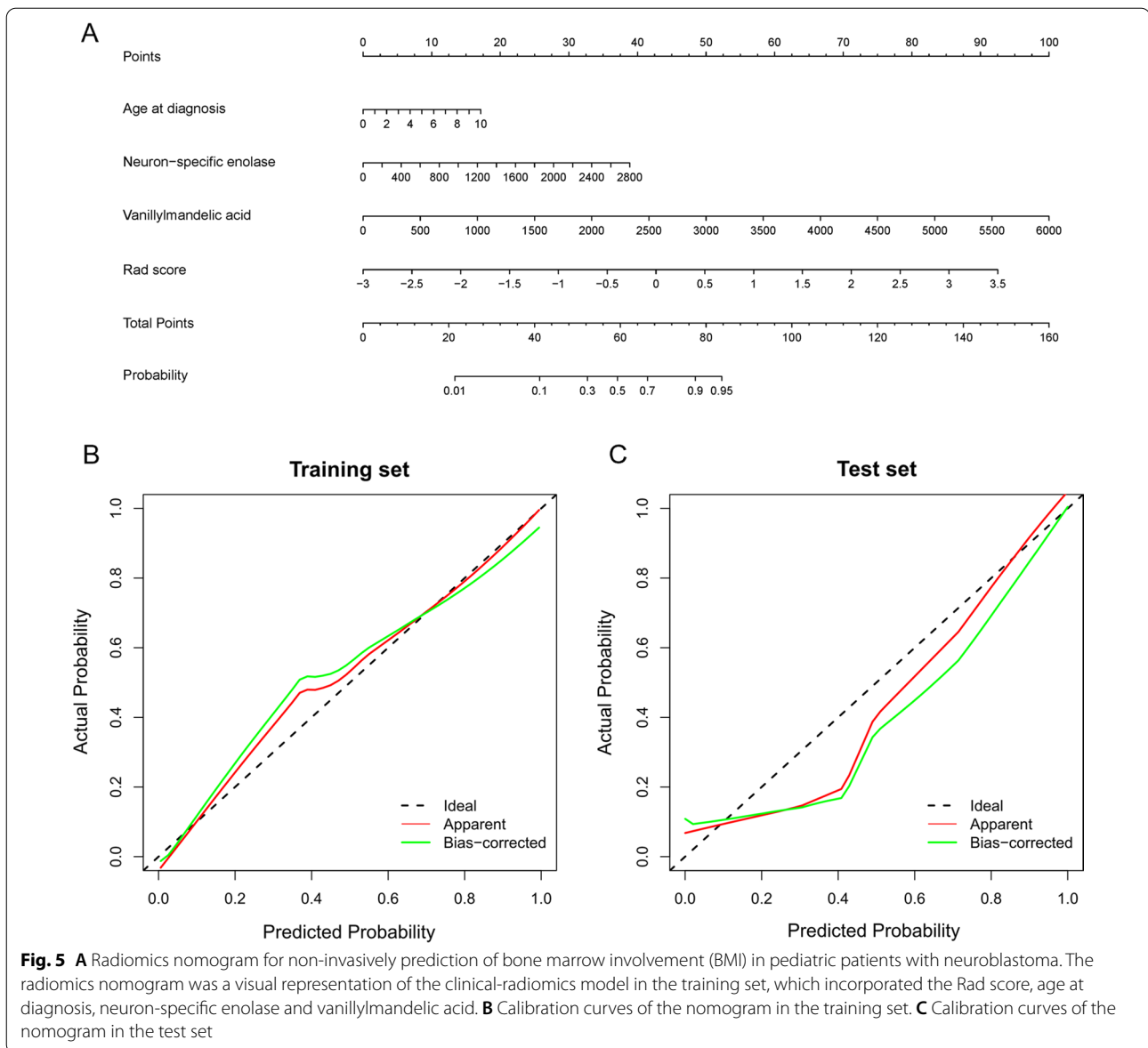


**Table 2** Univariate and multivariate logistic regression analysis of clinical characteristics for predicting the BMI in the training set

Characteristics	Univariate		Multivariate	
	OR (95% CI)	p value	OR (95% CI)	p value
Age at diagnosis (years)	1.547 (1.219, 1.962)	<0.001	1.551 (1.184, 2.031)	0.001
Gender	2.500 (1.079, 5.792)	0.033	NA	NA
Maximum diameter(cm)	1.215 (1.065, 1.387)	0.004	NA	NA
NSE (ng/mL)	1.003 (1.002, 1.005)	<0.001	1.003 (1.002, 1.005)	<0.001
Ferritin (ng/mL)	1.007 (1.003, 1.011)	<0.001	NA	NA
LDH (U/L)	1.000 (1.000, 1.001)	0.047	NA	NA
VMA ( $\mu\text{mol/L}$ )	1.002 (1.000, 1.003)	0.010	1.002 (1.001, 1.003)	0.006
HVA ( $\mu\text{mol/L}$ )	1.003 (0.999, 1.006)	0.161	NA	NA
SUVmax	1.309 (0.860, 1.991)	0.403	NA	NA
SUVmean	1.309 (0.860, 1.991)	0.209	NA	NA
MTV (mL)	1.003 (1.000, 1.006)	0.032	NA	NA
TLG	1.001 (1.000, 1.002)	0.029	NA	NA

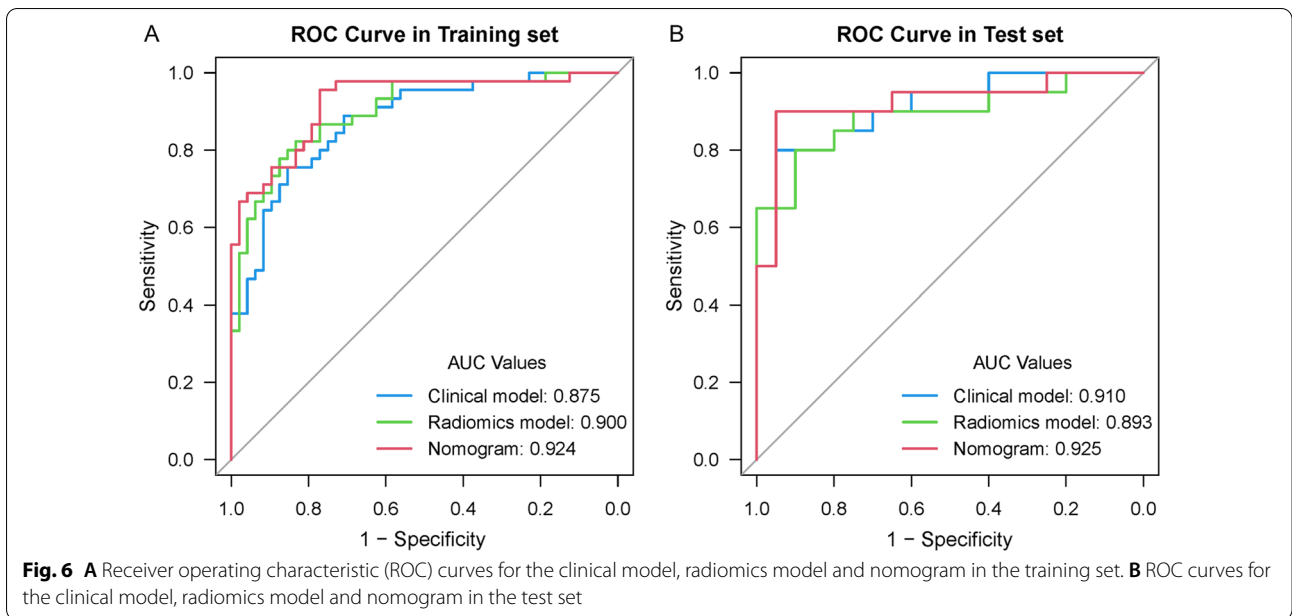
CI Confidence interval, HVA Homovanillic acid, LDH Serum lactate dehydrogenase, MTV Metabolic tumor volume, NA Not available, NSE Neuron-specific enolase, OR Odds ratio, TLG Total lesion glycolysis, VMA Vanillylmandelic acid



marker and can non-invasively provide the information for the diagnosis, improve the differential diagnosis, the classification of risk and staging, efficacy assessment, and prognosis of tumors [30].  $^{18}\text{F}$ -FDG PET/CT has the advantages of superior spatial resolution, high sensitivity, lesion semi-quantification, improved tumor-to-background contrast, and is widely used in the evaluation of pediatric neuroblastoma and metastasis [31]. A study compared different imaging modalities in 51 patients with high-risk neuroblastoma and concluded that  $^{18}\text{F}$ -FDG PET/CT is highly effective in identifying neuroblastoma for revealing small lesions, and for delineating the extent and localizing sites of disease [32]. In our study, a total of 2632 radiomics

features were extracted from both CT and PET images. Finally, twenty-five radiomics features based on the  $^{18}\text{F}$ -FDG PET/CT were selected by LASSO regression. The twenty-five radiomics features were used to construct the radiomics model and demonstrated a favorable ability to predict BMI in both the training and test sets. The radiomics model achieved an AUC of 0.900 in the training set and 0.893 in the test set in predicting BMI in children with neuroblastoma. Of the twenty-five radiomics features, the majority of selected features were wavelet features (18/25). It was indicated that features extracted from the images transformed by wavelet filter played an important role in the radiomics model. The wavelet filter can decompose special patterns hidden



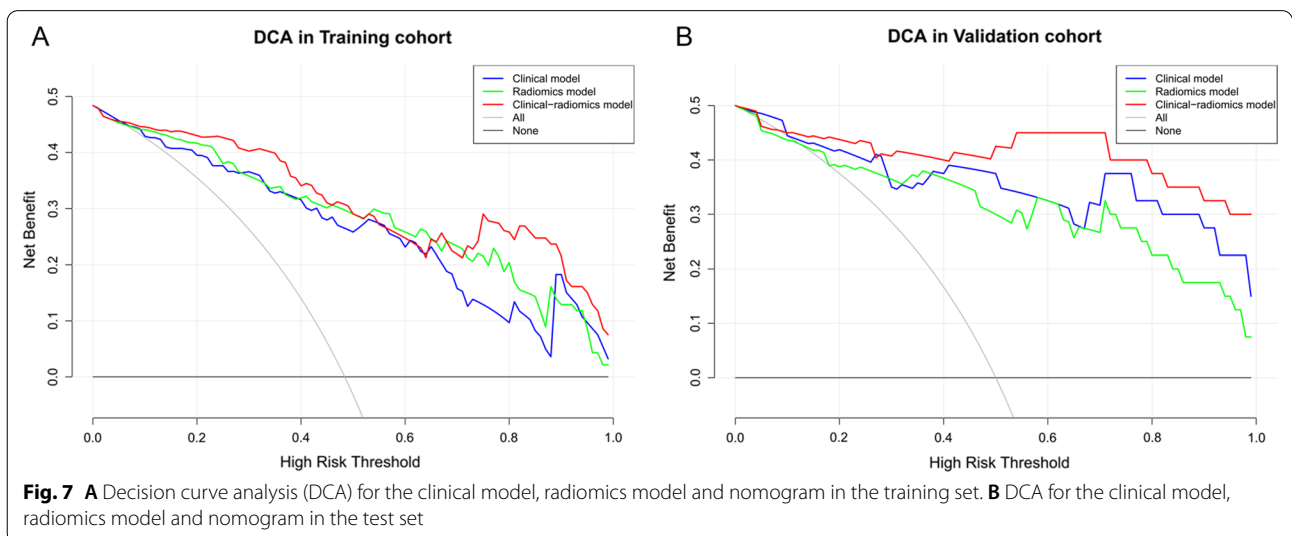


in the mass of data and the wavelet features may better explore tumor heterogeneity [21].

In addition to radiomics analysis, we also evaluated the value of clinical characteristics in predicting BMI. The age at diagnosis, NSE and VMA were identified as the independent predictors of BMI by univariate and multivariate logistic regression analyses. The children with age at diagnosis  $\geq 18$  months had a significantly higher risk of recurrence than those with age  $< 18$  months [33]. And for patients aged  $\geq 18$  months at diagnosis, there is a clear correlation between worse outcomes with the increasing metastatic burden (including BMI) [4]. NSE, a specific isoenzyme of the glycolytic enzyme enolase, is highly expressed in neurons and peripheral neuroendocrine

cells. Previous studies indicated that serum NSE levels  $\geq 100$  ng/mL were associated with a poor outcome [34]. Neuroblastoma can synthesize and secrete catecholamines and VMA is increased in the urine of children with neuroblastoma. Thus, the serum levels of NSE and urine levels of VMA are considered characteristic tumor markers of neuroblastoma [33], which can assess the condition, predict the effect of treatment and evaluate the prognosis of children with neuroblastoma [34].

Due to heterogeneity of clinical presentation of neuroblastoma, this disease is divided into clinically distinct subgroups, high, intermediate, and low-risk groups, based on different parameters, including the extent of the disease (whether or not with BMI). According to the INSS,



neuroblastoma was staged as stages 1, 2, 3, 4 and 4S. Tumors with dissemination to distant lymph nodes, bone, bone marrow, liver, skin and other organs were defined as stage 4. Of the stage 4 neuroblastoma patients, 78% have BMI. The spread of tumor cells to bone marrow is a grim prognostic factor in neuroblastoma patients, with a low 5-year event-free survival rate (29%) [4]. Therefore, BMI, age at diagnosis, NSE and VMA are all associated with poor prognosis in neuroblastoma. The present study demonstrated that the age at diagnosis, NSE and VMA as independent predictors of BMI. The clinical model included the three independent predictors with an AUC of 0.875 and 0.910 in the training and test sets, respectively.

Furthermore, we developed and validated an  $^{18}\text{F}$ -FDG PET/CT-based radiomics nomogram that incorporates the Rad score and independent predictors of BMI, which showed a preferable prediction of BMI in pediatric patients with neuroblastoma. Comparisons and evaluations of each model by DCA further demonstrated that the radiomics nomogram resulted in net benefits of providing more than the clinical model or radiomics model within a certain threshold probability range. The results showed that radiomics nomogram may provide the physician with an independent or auxiliary predictive tool to enhance the diagnostic efficiency for BMI in patients with neuroblastoma.

There were some limitations in this study. Our study was retrospective, which inevitably result in selection bias. Moreover, this was a single-center study and the sample size was relatively small, which makes it less generalizable to other centers, therefore, the clinical application and generalization of the model still need to be further improved and validated by multicenter studies with a larger sample size.

## Conclusions

In conclusion, the  $^{18}\text{F}$ -FDG PET/CT-based radiomics nomogram which incorporates Rad score and independent clinical risk factors (including the age at diagnosis, NSE, and VMA) showed satisfactory value for the prediction of the BMI in pediatric patients with neuroblastoma in this preliminary study, and larger series are required to confirm this study's results. As a non-invasive quantitative method, it holds the potential to assess the prognosis of the patients and assist in decision-making and further management of neuroblastoma.

## Abbreviations

AUC: Area under the curve; BMI: Bone marrow involvement; CI: Confidence interval; DCA: Decision curve analysis; HVA: Homovanillic acid; ICC: Intraclass correlation coefficient; INSS: International Neuroblastoma Staging System; LASSO: Least absolute shrinkage and selection operator; LDH: Lactate dehydrogenase; MTV: Metabolic tumor volume; NSE: Neuron-specific enolase; OR: Odds Ratio; ROC: Receiver operating characteristic; ROI: Regions of interest; TLG: Total lesion glycolysis; VMA: Vanillylmandelic acid.

## Supplementary Information

The online version contains supplementary material available at <https://doi.org/10.1186/s13244-022-01283-8>.

**Additional file 1.** Complete dataset.

**Additional file 2. Supplementary Fig. 1** The selected twenty-five features and their coefficients, and the formula for the Rad score. **Supplementary Table 1** The performance of the clinical-radiomics model by the different machine learning methods in the training and test sets.

## Acknowledgements

The authors thank the staff of the Department of Nuclear Medicine, Beijing Friendship Hospital, Capital Medical University, Beijing 100050, China for their selfless and valuable assistance.

## Author contributions

JY, LF and WW: conceptualization; XY, XL, YK, CW and DS: methodology; XY, CW and DS: software; LF, XL, YK and CW: validation; XL, YK, HZ and WW: formal analysis; LF, XY, XL, YK and CW: investigation; LF, XL, YK, and DS: data curation; LF, XY, XL, YK, CW, DS, HZ, WW and JY: writing—original draft preparation; LF, XY, XL, YK, CW, DS, HZ, WW and JY: writing—review and editing; LF, XY, XL, HZ and JY: visualization; WW and JY: supervision. All authors read and approved the final manuscript.

## Funding

This research was funded by Capital's Funds for Health Improvement and Research (No. 2020-2-2025), National Natural Science Foundation of China (No. 81971642, 82001861, 82102088), National Key Research and Development Plan (No. 2020YFC0122000).

## Availability of data and materials

The datasets analyzed during the current study are available from the corresponding author on reasonable request.

## Declarations

### Ethics approval and consent to participate

This retrospective study was approved by the institutional review board and waived the requirement for written informed consent.

### Consent for publication

Not applicable.

### Competing interests

The authors declare that they have no competing interests.

### Author details

<sup>1</sup>Department of Nuclear Medicine, Beijing Friendship Hospital, Capital Medical University, 95 Yong An Road, Xi Cheng District, Beijing 100050, China. <sup>2</sup>Sinounion Medical Technology (Beijing) Co., Ltd., Beijing 100192, China. <sup>3</sup>Department of Biomedical Engineering, School of Medicine, Tsinghua University, Beijing 100084, China.

Received: 12 June 2022 Accepted: 7 August 2022

Published online: 04 September 2022

## References

- Laut AK, Dorneburg C, Furstberger A et al (2022) CHD5 inhibits metastasis of neuroblastoma. *Oncogene* 41:622–633. <https://doi.org/10.1038/s41388-021-02081-0>
- Feng L, Qian L, Yang S et al (2022) Prediction for Mitosis-Karyorrhexis index status of pediatric neuroblastoma via machine learning based  $^{18}\text{F}$ -FDG PET/CT radiomics. *Diagnostics (Basel)*. <https://doi.org/10.3390/diagnostics12020262>

3. Yue ZX, Xing TY, Zhao W et al (2022) MYCN amplification plus 1p36 loss of heterozygosity predicts ultra high risk in bone marrow metastatic neuroblastoma. *Cancer Med*. <https://doi.org/10.1002/cam4.4583>
4. Morgenstern DA, London WB, Stephens D et al (2016) Prognostic significance of pattern and burden of metastatic disease in patients with stage 4 neuroblastoma: a study from the International Neuroblastoma Risk Group database. *Eur J Cancer* 65:1–10. <https://doi.org/10.1016/j.ejca.2016.06.005>
5. Liu J, Li C, Yang X et al (2022) The diagnostic value of <sup>18</sup>F-FDG PET/CT bone marrow uptake pattern in detecting bone marrow involvement in pediatric neuroblastoma patients. *Contrast Media Mol Imaging* 2022:7556315. <https://doi.org/10.1155/2022/7556315>
6. Burchill SA, Beiske K, Shimada H et al (2017) Recommendations for the standardization of bone marrow disease assessment and reporting in children with neuroblastoma on behalf of the International Neuroblastoma Response Criteria Bone Marrow Working Group. *Cancer* 123:1095–1105. <https://doi.org/10.1002/ncr.30380>
7. Cohn SL, Pearson AD, London WB et al (2009) The international neuroblastoma risk group (INRG) classification system: an INRG Task Force report. *J Clin Oncol* 27:289–297. <https://doi.org/10.1200/JCO.2008.16.6785>
8. Monclair T, Brodeur GM, Ambros PF et al (2009) The international neuroblastoma risk group (INRG) staging system: an INRG Task Force report. *J Clin Oncol* 27:298–303. <https://doi.org/10.1200/JCO.2008.16.6876>
9. Sharp SE, Shulkin BL, Gelfand MJ et al (2009) <sup>123</sup>I-MIBG Scintigraphy and <sup>18</sup>F-FDG PET in Neuroblastoma. *J Nucl Med* 50:1237–1243. <https://doi.org/10.2967/jnumed.108.060467>
10. Abila O, Friedman J, Doyle J (2008) Performing bone marrow aspiration and biopsy in children: Recommended guidelines. *Paediatr Child Health* 13:499–501. <https://doi.org/10.1093/pch/13.6.499>
11. Zapata CP, Cuglievan B, Zapata CM et al (2018) PET/CT versus bone marrow biopsy in the initial evaluation of bone marrow infiltration in various pediatric malignancies. *Pediatr Blood Cancer*. <https://doi.org/10.1002/pbc.26814>
12. Ak M, Toll SA, Hein KZ et al (2022) Evolving role and translation of radiomics and radiogenomics in adult and pediatric neuro-oncology. *AJNR Am J Neuroradiol* 43:792–801
13. Mayerhoefer ME, Riedl CC, Kumar A et al (2020) [18F]FDG-PET/CT radiomics for prediction of bone marrow involvement in mantle cell lymphoma: a retrospective study in 97 patients. *Cancers*. <https://doi.org/10.3390/cancers12051138>
14. Han EJ, O JH, Yoon H et al (2022) Comparison of FDG PET/CT and bone marrow biopsy results in patients with diffuse large B cell lymphoma with subgroup analysis of PET radiomics. *Diagnostics* (Basel). <https://doi.org/10.3390/diagnostics12010222>
15. Cook GJ, Yip C, Siddique M et al (2013) Are pretreatment <sup>18</sup>F-FDG PET tumor textural features in non-small cell lung cancer associated with response and survival after chemoradiotherapy? *J Nucl Med* 54:19–26. <https://doi.org/10.2967/jnumed.112.107375>
16. Kenawy MA, Khalil MM, Abdelgawad MH et al (2020) Correlation of texture feature analysis with bone marrow infiltration in initial staging of patients with lymphoma using <sup>18</sup>F-fluorodeoxyglucose positron emission tomography combined with computed tomography. *Pol J Radiol* 85:e586–e594. <https://doi.org/10.5114/pjr.2020.99833>
17. Boellaard R, Delgado-Bolton R, Oyen WJ et al (2015) FDG PET/CT: EANM procedure guidelines for tumour imaging: version 2.0. *Eur J Nucl Med Mol Imaging* 42:328–354. <https://doi.org/10.1007/s00259-014-2961-x>
18. Stauss J, Franzius C, Pfluger T et al (2008) Guidelines for <sup>18</sup>F-FDG PET and PET-CT imaging in paediatric oncology. *Eur J Nucl Med Mol Imaging* 35:1581–1588. <https://doi.org/10.1007/s00259-008-0826-x>
19. Leijenaar RT, Nalbantov G, Carvalho S et al (2015) The effect of SUV discretization in quantitative FDG-PET Radiomics: the need for standardized methodology in tumor texture analysis. *Sci Rep* 5:11075. <https://doi.org/10.1038/srep11075>
20. Tixier F, Le Rest CC, Hatt M et al (2011) Intratumor heterogeneity characterized by textural features on baseline <sup>18</sup>F-FDG PET images predicts response to concomitant radiochemotherapy in esophageal cancer. *J Nucl Med* 52:369–378. <https://doi.org/10.2967/jnumed.110.082404>
21. Zhou Y, Zhou G, Zhang J et al (2022) DCE-MRI based radiomics nomogram for preoperatively differentiating combined hepatocellular-cholangiocarcinoma from mass-forming intrahepatic cholangiocarcinoma. *Eur Radiol*. <https://doi.org/10.1007/s00330-022-08548-2>
22. Chen X, Wang H, Huang K et al (2021) CT-based radiomics signature with machine learning predicts MYCN amplification in pediatric abdominal neuroblastoma. *Front Oncol* 11:687884. <https://doi.org/10.3389/fonc.2021.687884>
23. Xv Y, Lv F, Guo H et al (2021) Machine learning-based CT radiomics approach for predicting WHO/ISUP nuclear grade of clear cell renal cell carcinoma: an exploratory and comparative study. *Insights Imaging* 12:170. <https://doi.org/10.1186/s13244-021-01107-1>
24. Zhou HF, Han YQ, Lu J et al (2019) Radiomics facilitates candidate selection for irradiation stents among patients with unresectable pancreatic cancer. *Front Oncol* 9:973. <https://doi.org/10.3389/fonc.2019.00973>
25. Lee HA, Chen KW, Hsu CY (2022) prediction model for pancreatic cancer—a population-based study from NHIRD. *Cancers* (Basel). <https://doi.org/10.3390/cancers14040882>
26. Van Griethuysen JJM, Fedorov A, Parmar C et al (2017) Computational radiomics system to decode the radiographic phenotype. *Cancer Res* 77:e104–e107. <https://doi.org/10.1158/0008-5472.CAN-17-0339>
27. Badr S, Kotb M, Elahmady MA et al (2018) Predictive value of FDG PET/CT versus bone marrow biopsy in pediatric lymphoma. *Clin Nucl Med* 43:e428–e438. <https://doi.org/10.1097/rlu.0000000000002315>
28. Feng L, Qian L, Yang S et al (2022) Clinical parameters combined with radiomics features of PET/CT can predict recurrence in patients with high-risk pediatric neuroblastoma. *BMC Med Imaging* 22:102. <https://doi.org/10.1186/s12880-022-00828-z>
29. Jie B, Hongxi Y, Ankang G et al (2022) Radiomics nomogram improves the prediction of epilepsy in patients with gliomas. *Front Oncol* 12:856359. <https://doi.org/10.3389/fonc.2022.856359>
30. Liu Z, Li M, Zuo C et al (2021) Radiomics model of dual-time 2-[<sup>18</sup>F]FDG PET/CT imaging to distinguish between pancreatic ductal adenocarcinoma and autoimmune pancreatitis. *Eur Radiol* 31:6983–6991. <https://doi.org/10.1007/s00330-021-07778-0>
31. Lee JW, Cho A, Yun M et al (2015) Prognostic value of pretreatment FDG PET in pediatric neuroblastoma. *Eur J Radiol* 84:2633–2639. <https://doi.org/10.1016/j.ejrad.2015.09.027>
32. Kushner BH, Yeung HW, Larson SM et al (2001) Extending positron emission tomography scan utility to high-risk neuroblastoma: fluorine-18 fluorodeoxyglucose positron emission tomography as sole imaging modality in follow-up of patients. *J Clin Oncol* 19:3397–3405. <https://doi.org/10.1200/jco.2001.19.14.3397>
33. Li F, Zhang W, Hu H et al (2022) Factors of recurrence after complete response in children with neuroblastoma: a 16-year retrospective study of 179 cases. *Cancer Manag Res* 14:107–122. <https://doi.org/10.2147/CMAR.S343648>
34. Li J, Liu X, Chen M et al (2021) Values of serum CA125, NSE and 24-hour urine VMA in diagnosis and prediction of treatment of paediatric neuroblastoma. *Int J Clin Pract* 75:e14932. <https://doi.org/10.1111/ijcp.14932>

## Publisher's Note

Springer Nature remains neutral with regard to jurisdictional claims in published maps and institutional affiliations.